2022-01-5026 Published 13 Apr 2022

Prediction of Electric Vehicle Transmission Efficiency Using a New Thermally Coupled Lubrication Model

Joseph F. Shore and Athanasios I. Christodoulias Imperial College London

Anant S. Kolekar and Frances E. Lockwood Valvoline

Amir Kadiric Imperial College London

Citation: Shore, J.F., Christodoulias, A.I., Kolekar, A.S., Lockwood, F.E. et al., "Prediction of Electric Vehicle Transmission Efficiency Using a New Thermally Coupled Lubrication Model," SAE Technical Paper 2022-01-5026, 2022, doi:10.4271/2022-01-5026.

Received: 23 Oct 2021 Revised: 12 Jan 2022 Accepted: 09 Mar 2022

Abstract

We present a new method to predict the power losses in electric vehicle (EV) transmission systems using a thermally coupled gearbox efficiency model. Friction losses in gear teeth contacts are predicted using an iterative procedure to account for the thermal coupling between the tooth temperature, oil viscosity, film thickness, friction, and oil rheology during a gear mesh cycle. Crucially, the prediction of the evolution of the coefficient of friction (COF) along the path of contact incorporates measured lubricant rheological parameters as well as measured boundary friction. This allows the model to differentiate between nominally similar lubricants in terms of their impact on EV transmission efficiency. Bearing and gear churning losses are predicted using existing empirical relationships. The effects of EV motor cooling and heat transfers in the heat exchanger on oil temperature are considered. Finally, heat transfer to the surroundings is accounted for so that the evolution of gearbox temperature over any given drive cycle can be predicted. The general approach presented here is applicable to any automotive gearbox while incorporating features specific to EVs. The model predictions are compared to real road measurements made on a popular current EV, and good agreement is shown over a range of road conditions. It should be noted that at high input speeds, the current model somewhat overpredicts the gearbox losses due to limitations in existing empirical bearing and churning loss models. Analyses of transmission losses breakdown at constant input power show that at low speeds/high torques, it is the losses in the gear meshes and high-load bearings that are most significant whereas at high speeds/low torques the losses in high-speed input shaft bearings, as well as gear churning losses, become more important. It is shown that the gearbox losses can account for 15-25% of the overall power losses in an EV depending on road conditions; a much higher proportion than in an internal combustion engine (ICE) vehicle, thus demonstrating that reducing transmission losses offers an important avenue for improving EV efficiency. Finally, the influence of oil properties on EV transmission losses is demonstrated by applying the model to predict losses over the Worldwide Harmonized Light Vehicles Test Procedure (WLTP) drive cycle. The presented model can help to optimize both gearbox design and lubricant properties to minimize EV transmission losses and hence improve EV range.

Keywords

Electric vehicle (EV), Transmissions, Efficiency, Gears

1. Introduction

Unlike internal combustion engines (ICEs), which have a maximum efficiency of around 40% due to thermodynamic limitations, modern electric motors (EMs) used in electric vehicles (EVs) typically operate with efficiencies in excess of 90% [1]. It may therefore be expected that the losses in EV transmissions, even if small in absolute terms, make up a much larger proportion of the overall vehicle power loss than is the case for an equivalent ICE-powered vehicle. This proportion has been shown to be in the region

of 15-20% of the EV total powertrain loss [2]. Therefore, improving our ability to predict EV transmission losses and subsequently reduce them through lubricant selection and gearbox design optimization presents an important way to improve the efficiency of EVs and extend their battery range.

Due to vastly different torque-speed characteristics of the prime mover, transmission designs in EVs are significantly different from those in ICE vehicles [3]. While an ICE idles around 800 rev/min and develops usable torque over a narrow engine speed range, an EM provides its maximum available torque close to stall and useful torque over a much wider speed range and at relatively high efficiencies [1]. These differences mean that while ICE-powered vehicles require a change gearbox to satisfy the road conditions, typical EVs can provide satisfactory performance with a single ratio transmission, typically with a reduction ratio of approximately 8:1, negating the need for a clutch and its associated auxiliary systems. However, given the high speeds of EMs employed in modern EVs, typical EV transmission must operate over a much wider range of input speeds than an ICE vehicle transmission, from zero to over ten thousand revolutions per minute. This presents competing challenges as the transmission and lubricant must be designed to operate efficiently and reliably across this entire range of conditions: in one extreme, the transmission and oil must cope with high torque/low speed conditions, which call for high viscosity oils, while in the other, high speeds/low torque conditions call for the use of low viscosity oils to control oil churning losses. In many systems where the same fluid is used to cool the EM as well to lubricate the gearbox, the thermal properties of the oil are also of paramount importance. Despite this, the current EVs commonly employ conventional automatic transmission fluids (ATFs), which are primarily designed to provide satisfactory frictional performance in automatic transmission systems rather than optimize performance over the wide range of tribological conditions present in EV transmissions [4].

Some recent studies [5, 6, 7, 8, 9, 10] have modeled the effects of implementing different transmission architectures in EVs, such as two-speed transmission instead of a more common single ratio. Multiple ratios have the benefit of allowing the motor to operate in a more efficient region over a wider range of road conditions. However, it is also recognized that the degree to which this can improve the EV efficiency is dependent on the vehicle duty cycle [6] and these studies implemented only simple models of gearbox efficiency. The addition of multiple stages introduces additional components such as shift elements which will act to increase transmission losses and vehicle weight which may offset any gains in operating motor efficiency.

Over the last few decades, there have been several notable studies of power losses in general geared transmissions, not necessarily in EV applications. Early work by Anderson et al. [11] used empirical formulae for meshing losses in a single spur gear pair, and also accounted for gear churning and bearing losses. These predictions agreed well with experimental results, but the range of conditions tested was relatively limited. Petry-Johnson et al. [12] investigated gear losses using an FZG test rig. They studied multiple lubricants and the effects of surface roughness and tooth number, finding that gear losses were most affected by the surface roughness and normal module while gear churning losses were most affected by viscosity. The work by Michaelis et al. [13] concurred with this finding that substantial energy savings could be made in wind turbine gearboxes through the use of lower viscosity oils. They also found that substantial reductions in bearing losses could be made in an automotive gearbox by optimizing bearing selection, although this was also highly temperature dependent. Numerical studies by Li and Kahraman [14] and Chang and Jeng [15] on single spur gear pairs also showed good agreement with the results from Petry-Johnson et al. [12].

A key difficulty in the prediction of gearbox losses is the thermal coupling between gear tooth temperature, oil film temperature, friction, and oil film thickness in gear teeth contacts. Owing to these difficulties, many relevant methods rely on relatively crude approximations such as a 20°C difference between the oil sump temperature and the gear tooth bulk temperature, or that the bulk temperature is equal to the sum of the sump temperature and a fraction of the maximum flash temperature during a mesh cycle [16]. Since oil temperature plays such a crucial role in determining friction losses during a mesh cycle, such assumptions are not suitable for accurate predictions of power losses and are unable to distinguish between two gear oils of the same grade in terms of their impact on gearbox power losses which is needed if gear oil selection is to be optimized. An additional complication in EV applications is that the gear oil is often used to also cool the EM. Therefore, this additional heat transfer must be accounted for when determining the oil properties needed for frictional and churning loss calculations.

More sophisticated treatments of gearbox temperatures include that of Changenet et al. [17] who modeled thermal coupling within a six-speed manual gearbox via a thermal network approach. This allowed for local changes in oil temperature to be accounted for when determining gear, bearing, and churning losses. The temperature predictions of this model generally showed good agreement with experimental results. This approach was further developed by Durand De Gevigney et al. [18] for an FZG rig, again showing close agreement to experiments. This study demonstrated that assuming the gearbox to be isothermal was unrealistic, with bulk temperatures of the gearbox components shown to vary significantly from that of the sump under certain conditions. It also highlighted the importance of the immersion depth of the gear in the oil sump reduction which reduces gear churning losses but also reduces the extent of gear cooling provided by the oil.

The gearbox efficiency model presented in this paper attempts to address some of the issues identified above as well as account for additional factors specific to EV applications with the aim of providing a useful tool to help in optimizing EV gearbox design and lubricant selection. This is achieved by (i) Employing a thermally coupled gear tooth lubrication model which accounts for transient tribological conditions in the tooth contacts during a mesh cycle and the interdependency of friction, gear tooth bulk temperatures, and oil film thickness: (ii) A more detailed consideration of relevant gearbox temperatures including gear tooth bulk temperature predictions accounting for heat produced in the tooth contacts and gear heat loss through convection and conduction as well as oil sump temperature for any given vehicle drive cycle; (iii)

Employing measured rheological properties for the specific oil under consideration so that the model can distinguish between two nominally same oils in terms of their impact on gearbox efficiency; (iv) Accounting for additional heat transfers due to oil being used to cool the EM in a manner employed in a typical current EV; (v) Making the model computationally efficient so that it can be applied to predict losses in any given vehicle drive cycle. In the present paper, the model is applied to a specific gearbox design found in a popular production EV and its predictions validated against measurements made on the vehicle under real road driving conditions. Finally, the model is used to analyze the breakdown of transmission losses and hence identify the dominant sources of power loss under different conditions as well as to illustrate the influence of oil properties on the power losses over a standardized drive cycle.

1.1. Transmission Power Losses

Transmission losses can be broadly divided into load-dependent losses, which include gear and bearing friction, and load-independent losses, which include gear and bearing oil churning, seal, and any auxiliary losses. This is illustrated in Figure 1.

1.1.1. Gear Friction

The key to determining the power loss in the gear mesh is the determination of the evolution of the COF along the path of contact during the mesh cycle. This problem is convoluted by the interdependency of friction, lubricant film thickness, and gear tooth bulk temperature, as well as the non-Newtonian behavior of the lubricants in the gear tooth contacts which typically operate under elastohydrodynamic (EHL) and mixed lubrication regimes [19, 20, 21]. The heat generated by the contact friction increases the tooth bulk temperature which reduces the oil viscosity in the contact inlet and hence the oil film thickness; this, in turn, changes the COF and power losses [22, 23]. Any procedure to determine these quantities must therefore be iterative and must also account for the variable contact conditions along the path of contact during a mesh cycle.

Many gear efficiency models [24, 25, 26, 27] rely on the assumption of a constant COF along the contact path and only consider the lubricant properties at the contact inlet [23, 28]. In reality, the problem is highly transient throughout a single mesh cycle due to the involute geometry of gear teeth, where the relative radii of curvature and load change continuously along the path of contact [23, 29]. This results in changes in COF due to continuously changing contact pressure and slide-roll ratio (SRR), resulting in sliding friction falling to zero at the pitch point where the contact is in pure rolling conditions. Other models, such as those proposed by Benedict and Kelley [30] and by Xu [28] describe the change in local COF along the contact path by using empirical fits derived from experimental results and computational models, respectively. The Benedict and Kelley empirical relationship is widely used and offers an easy-to-implement approach to a complex problem but suffers from inaccuracies not least at low SRRs near the pitch point, where it fails to predict the drop in COF to near zero [30]. This is a common issue with many other empirical fits, as explained by Fernandes [31].

While these models provide reasonably accurate approximations of the operation of the gear pair, they only consider nominal lubricant properties, such as viscosity, and do not account for lubricant rheology [28, 31]. The failure to account for rheology is a significant shortcoming as this strongly influences the COF in the gear tooth contacts [21]. This greatly inhibits the applicability of these models to gearbox optimization, such as the selection of lubricants to improve the efficiency of transmission.

1.1.2. Bearing Losses

Bearing losses contribute a major proportion of overall power losses in a transmission [23, 32]. Total bearing losses include rolling resistance, sliding friction, seal losses, and drag losses [32, 33, 34, 35, 36]. Many studies on the prediction of transmission losses [13, 23, 24, 37, 38, 39] implement the SKF bearing loss model [33, 34]. This model has the advantage of requiring only a few input parameters regarding operating conditions, bearing type, and geometry.

The literature describing this model [33, 34] makes it clear that, due to the treatment of bearing drag losses, the model should only be used at bearing speeds up to $N \cdot d_m = 0.5 \times 10^6$ mm-rev/min, where $N{\cdot}d_m$ is the product of bearing speed in revolutions per minute and bearing mean diameter in millimeters (mm). At higher $N{\cdot}d_m$ values, the model overestimates the drag losses, and SKF do not recommend its use under such conditions. This may have important implications for the prediction of losses in EV transmissions under certain conditions since the input speeds in modern EVs can be over 10,000 rev/min.

1.1.3. Churning Losses

Most automotive transmissions employ a splash or sump lubrication system to supply oil to the gears and bearings. In such a system, gears are partially submerged in an oil bath and as they rotate the teeth pick up

FIGURE 1 Sources of transmission losses.

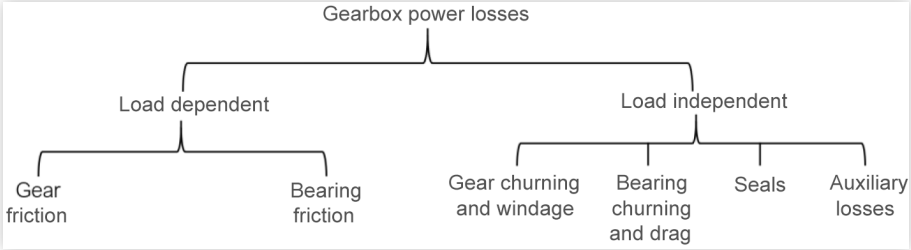

and throw the oil around the inside of the casing, thereby lubricating and cooling gears and bearings. A downside of this is that as speed increases, the energy spent on churning the lubricant in this way increases drastically [40]. In EV transmissions, where speeds will often reach more than 10,000 rev/min, the contribution of churning losses can be especially important. Reducing churning losses is a complex optimization problem as decreasing immersion depth will reduce churning losses [25] but will reduce the effectiveness of gear cooling by the lubricant [41], thereby decreasing oil film thickness in gear teeth contacts and potentially increasing the risk of component failures [25]. There are a number of empirically derived formulae for estimating churning losses [42, 43, 44]. The experimentally derived fits proposed by Changenet and Velex [45], developed using dimensional analysis, are employed in this paper.

2. Model Description

The gearbox power loss model described here considers all main sources of losses, namely, gear tooth contact friction, losses, gear churning losses, and total bearing losses.

2.1. Thermally Coupled Gear Lubrication Model

The current model accounts for the coupling between oil temperature, bulk gear tooth temperature, lubricant properties, film thickness, and COF by using an iterative procedure to calculate these values at many points along the contact path during the mesh cycle while also accounting for lubricant rheology.

The contact pressure at each point along the contact path is determined using Hertzian formulae. In spur gears, this is done by approximating the line contact between the gear teeth as the contact between two cylinders of radii is equal to the radii of curvature of the involutes at that point. In helical gears, a conical approximation is used.

2.1.1. EHL Traction Prediction

The model makes use of an Eyring rheology model, which relates the shear rate $\dot{\gamma}$ to shear stress τ and viscosity η_p via the Eyring stress τ_0, using Equation 1.

$$\dot{\gamma} = \frac{\tau_0}{\eta_p} \sinh\left(\frac{\tau}{\tau_0}\right) \quad \text{Eq. (1)}$$

The shear rate is defined in Equation 2 as the ratio of sliding speed U_s to the central film thickness h_c, calculated using Chittenden's empirical regressions [23, 46, 47], assuming that there is a constant velocity gradient in the central film area [23, 48]. Shear thinning is not considered in the current model.

$$\dot{\gamma} = \frac{U_s}{h_c} \quad \text{Eq. (2)}$$

The in-contact viscosity η_p is determined using the temperature and pressure corrected Roelands equation (Equation 3).

$$\frac{\eta_p}{\eta_\infty} = \exp\left[\ln\left(\frac{\eta_r}{\eta_\infty}\right) \cdot \left(1 + \frac{p}{p_r}\right)^z \cdot \left(\frac{T_r + 135}{T + 135}\right)^{S_0}\right] \quad \text{Eq. (3)}$$

This equation relates the in-contact viscosity η_p at a given pressure p and temperature T to a reference viscosity η_r found at reference temperature T_r and atmospheric pressure p_r [23]. The value z is lubricant specific and can be determined through a series of traction experiments, as explained further in Section 3.1.

The regime in which the contact is operating is determined using the algorithm developed by Olver and Spikes [19], shown in Figure 2, which is based on three nondimensional parameters, the Deborah number D_0, the nondimensional strain rate S, and the nondimensional limiting shear stress τ_c^*. These are defined by parameters relating to the operating conditions and lubricant properties in Equations 4, 5, and 6, respectively [19, 23].

FIGURE 2 Adapted flowchart of Olver and Spikes' [19] algorithm to determine the lubrication regime.

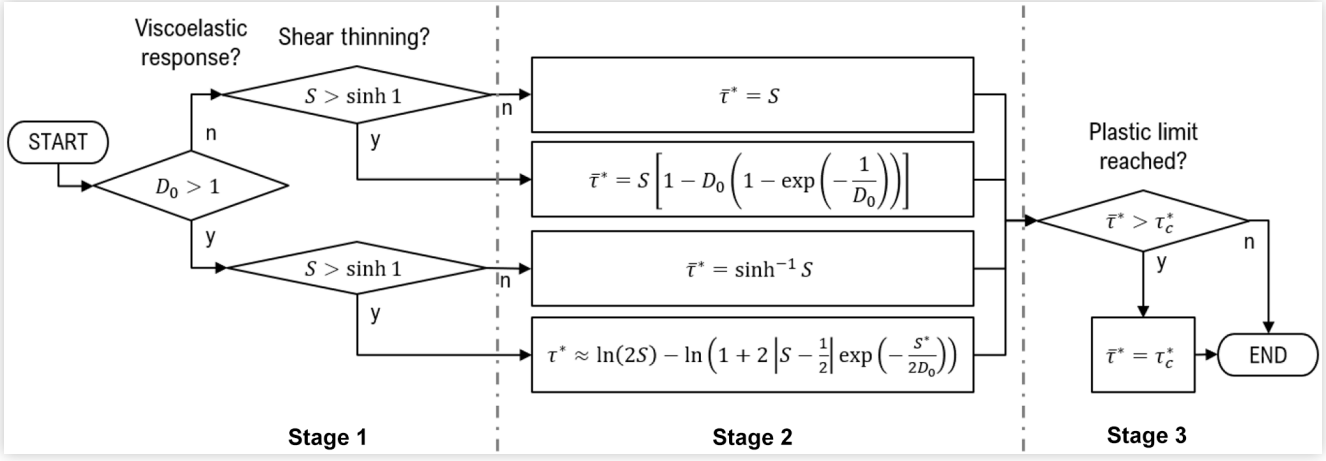

Data taken from Ref. [19], © SAE International

$$D_0 = \frac{\eta_0 U}{2\alpha_0 G_e} \quad \text{Eq. (4)}$$

$$S = \frac{\dot{\gamma}\eta_0}{\tau_0} \quad \text{Eq. (5)}$$

$$\tau_c^* = \frac{\tau_c}{\tau_0} \quad \text{Eq. (6)}$$

where η_0 is the inlet viscosity, U is the entrainment speed, α_0 is the Hertzian contact half-width in the rolling direction, G_e is the elastic shear modulus, and τ_c is the critical shear stress. All other symbols maintain their aforementioned definitions.

Once $\bar{\tau}^*$ is determined, the fluid COF can be calculated through Equation 7:

$$\mu_f = \frac{\bar{\tau}^* \tau_0}{\bar{p}} \quad \text{Eq. (7)}$$

To apply this procedure to calculate gear friction, it is necessary to determine the value of the Eyring stress at the oil temperature and contact pressure in the gear contact. To do this, the experimental procedure described in Section 3.1 is used to create a matrix of τ_0 values at various temperatures and pressures. Interpolation can then be used to determine the value of τ_0 at any operating conditions.

2.1.2. Friction in the Mixed Lubrication Regime Gears frequently operate in the mixed lubrication regime [23]. Therefore, the model takes into account the surface roughness of the gear by considering the lambda ratio Λ and the boundary COF μ_b by implementing the empirical Equation 8 described in [19, 49]:

$$\mu = \mu_f + \frac{\mu_b - \mu_f}{(1+\Lambda)^m} \quad \text{Eq. (8)}$$

where m is approximately equal to 2. This equation is used whenever the SRR is greater than 0.001, i.e., unless the gears are at the pitch point, where they operate under pure rolling. Here μ is taken to be equal to μ_f. The value of μ_b is determined experimentally as described in Section 3.2.

Once the COF is determined, the related power loss can be calculated from the load and sliding speed.

2.1.3. Thermal Coupling Thermal coupling in the gear contact is accounted for by the procedure illustrated in Figure 3.

The inner loop is an iterative procedure to determine the conditions within the contact at each point along the contact path. The outer loop increments along the contact path. The converged properties calculated at each point along the path of contact serve as the initial values for the convergence loop for the subsequent point.

FIGURE 3 Illustration of the iterative algorithm employed in the current model.

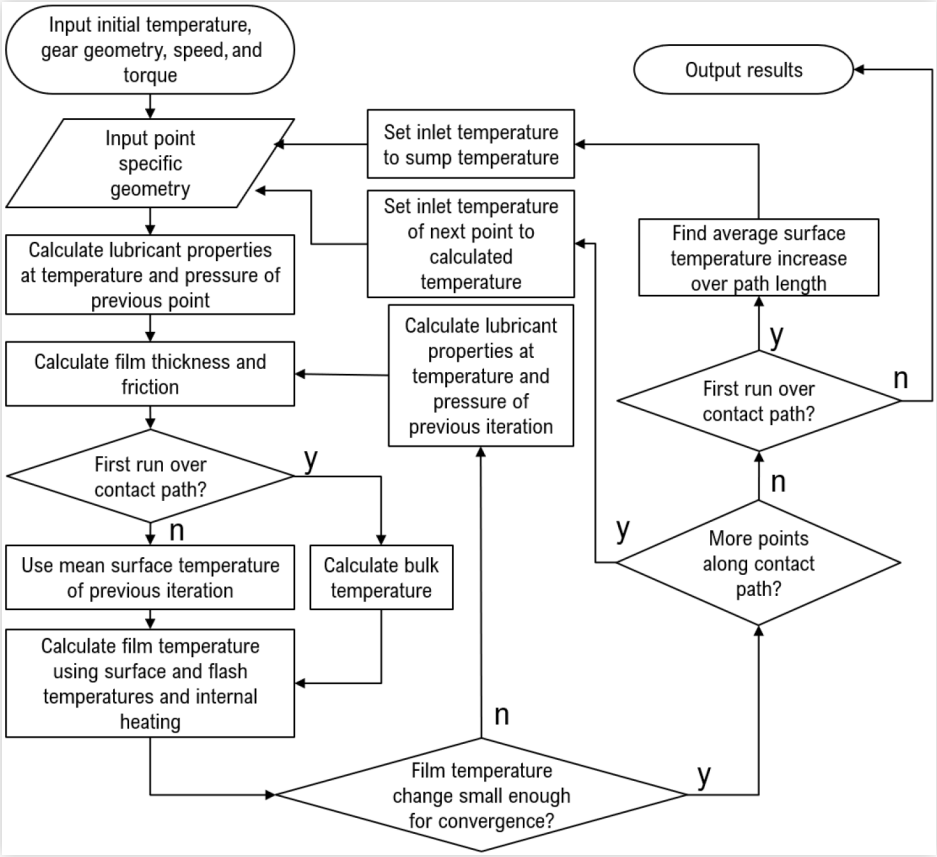

It can be seen that the conditions along the contact path are calculated twice, using different values for the gear tooth bulk temperature. First, the gear bulk temperature, calculated at each point, is used. In the second run, the average of the values calculated in the initial run is used instead. This is approach is more realistic than using the initially calculated instantaneous tooth bulk temperature because significant temperature variation from point to point in steel gears is unrealistic due to the speed at which the path of contact is traversed [23].

In the inner loop, the thermal coupling in the gear mesh is accounted for by solving the thermal network developed by Olver and Spikes [19], shown in Figure 4, to find the oil temperature T_{oil}. The algorithm then checks the difference between this value and the one used to calculate the COF. If the difference is too great for convergence, the COF is recalculated using the new value for temperature. The procedure is repeated until the convergence criterion is satisfied. The thermal network accounts for the complexities associated with the multitude of methods of heat dissipation and the continuously changing conditions along the path of contact by treating the system as a series of thermal resistances, representing the fluid half-film, the transient thermal resistance of the gear surface, and the steady-state thermal resistance of the gear body [19, 23, 50]. In Figure 4, T_A represents the temperature of the oil away from the contact. This was taken to be equal to the sump temperature in the splash-lubricated second stage and the temperature of the oil spray in the spray-lubricated first stage.

The heat partition into each gear can be calculated by equating the mean oil film temperature on the two surfaces, following Olver [19]. This leads to the heat partition fraction α_h, defined by Equation 9.

$$\alpha_h = \frac{1.06B_2 + \frac{h_c}{2k_{oil}A} + M_2}{1.06\left(B_1 + B_2\right) + \frac{h_c}{k_{oil}A} + \left(M_1 + M_2\right)} \qquad \text{Eq. (9)}$$

B_1 and B_2 are the transient thermal resistances of the two surfaces. The steady-state thermal resistances of Gears 1 and 2, M_1 and M_2 respectively, are determined by considering the steady-state thermal resistances of gear sides M_{sides} and the track M_{track} in parallel (Equation 10) [23, 50]:

$$M_{total} = \frac{1}{1/M_{track} + 1/M_{sides}} \qquad \text{Eq. (10)}$$

M_{sides} is estimated by approximating the gear as a thin disc, with a facewidth much smaller than its radius, and a thermal gradient restricted to the radial direction. As such, the standard solution for a circular cooling fin can be used, with the heat transfer coefficient (HTC) for forced convection being calculated using the standard solution for a laminar flow over a flat plate [23, 50]. For the track, the gear tooth is approximated as an infinite cylinder, with a facewidth much larger than its radius. This assumes that heat is lost through the track only [23, 50]. The HTC is calculated by assuming 1D transient conduction between the gear and the oil. Christodoulias [23] calculated the average rate of heat flow by considering the heat transfer over specific periods of time, either the time taken for a full gear rotation or the time that a tooth spends below the gear's nominal immersion depth, concluding that the latter approach was superior for splash-lubricated gears as it directly related the heat flow rate to the lubricant level.

In spray-lubricated gears, as is the case in the first stage of the real EV transmission analyzed in Section 2.4, heat transfer is expected to be enhanced as heat is constantly being removed from the teeth by the spray. Therefore, it was deemed more appropriate to consider that heat is transferred from the tooth throughout the time taken for a full gear rotation. Comparative tests using each method showed that the discrepancy in the prediction of the COF between the two methods is less than 1%.

Although this approach to determining the HTC provides a useful first-degree approximation, it fails to account for many complexities in the geometry and operation of the gears which act to enhance heat transfer [23, 50]. This is further discussed in Section 5.1.

Figure 5 shows examples of the output of the thermally coupled lubrication model along the path of contact for a set of 1:1 uncorrected spur gears using the measured rheology of an example gear oil. The combined R_q surface roughness of the gear teeth in this example is 300 nm. The absolute values of COF in this particular example (0.04 to 0.55) are typical of gear lubrication and reflect the imposed mixed lubrication conditions. The exact value at any particular point in the mesh cycle is affected by the load and SRR at that location and COF falls to zero at the pitch point where the gear teeth operate under pure rolling conditions, resulting in a decrease in oil temperature. The minimum film thickness is somewhere near the first point of the single-pair tooth contact region. In the double-pair contact region, the load is determined by linear interpolation between zero and the load in single-pair contact. The predicted film thickness at the extremes of the contact

FIGURE 4 The thermal network accounting for heat partition between a gear pair, adapted from [19].

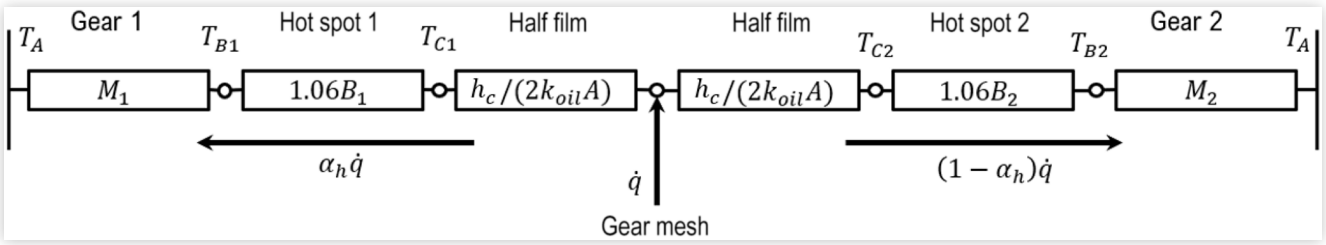

Based on Ref. [19]. © SAE International

FIGURE 5 Example prediction of COF, Λ ratio, and contact temperature along the path of contact for an example pair of 1:1 uncorrected spur gears; 200 Nm, 1500 rev/min, 50°C sump temperature, 300 nm combined R_q surface roughness.

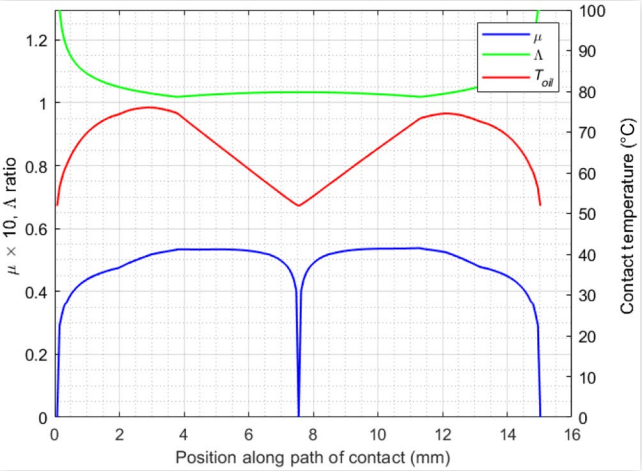

path appears to increase rapidly, but it should be noted that predictions in this region are unreliable as it is difficult to model the exact contact conditions when the teeth first come into contact as they are highly dependent on lubricant entrainment and exact aspects of the gear tooth geometry such as tip reliefs, which are not considered in this example.

2.2. Bearing Losses

The SKF model [33, 34] defines the resistive moment within a bearing with Equation 11, as the sum of four frictional moments: M_{rr}, M_{sl}, M_{seal}, and M_{drag}, corresponding to rolling resistance, sliding friction, seal friction, and hydrodynamic drag, respectively [33, 34].

$$M = \phi_{ish}\phi_{rs}M_{rr} + M_{si} + M_{seal} + M_{drag} \qquad \text{Eq. (11)}$$

ϕ_{ish} is the inlet shear heating reduction factor and ϕ_{rs} is the kinematic replenishment factor. This accounts for the hysteresis of the lubricant due to its viscosity. The result of this hysteresis is that lubricant expulsed from the contact by a rolling element does not have adequate time to reflow into the contact before the next element passes by. The magnitude of the loss sources and factors can be determined from the operating conditions and constants related to the bearing geometry and type and the lubrication conditions using tables provided by SKF [33, 34]. The bearing oil level was assumed to be half of the diameter of the rolling element, as the level recommended by SKF [34].

The axial and radial loads on the bearings are determined by solving free-body diagrams of the shafts. Point loads and light components were assumed. In automotive applications, these assumptions are justifiable as facewidth ratios tend to be small and the loads resulting from the shaft torque are expected to be much higher than that from the weight of the components.

As previously stated, SKF do not recommend using this model at speeds where $N{\cdot}d_m$ exceeds $N \cdot d_m = 0.5 \times 10^6$ mm · rev/min. Once available, an improved model for high-speed applications can be substituted into the overall model.

2.3. Churning Losses

To determine the churning losses within the transmission, the empirical model developed by Changenet and Velex [45] has been implemented. This model implements Equation 12 for the churning torque C_{ch} on a single gear rotating in a sump in terms of a nondimensional churning torque C_m.

$$C_{ch} = \frac{\rho}{2}\omega^2 S_m R_p^3 C_m \qquad \text{Eq. (12)}$$

where S_m is the submerged surface area of the gear when stationary. The nondimensional churning torque is described by the empirically derived Equation 13.

$$C_m = \psi_1 \left(\frac{m_n}{D_p}\right)^{\psi_2} \left(\frac{b}{D_p}\right)^{\psi_3} \left(\frac{h}{D_p}\right)^{\psi_4} \left(\frac{V_0}{D_p^3}\right)^{\psi_5} Re^{\psi_6} Fr^{\psi_7} \qquad \text{Eq. (13)}$$

where Re and Fr are the Reynolds and Froude numbers, respectively, and the values of $\psi_{1\text{-}7}$ depend on the critical Reynolds number Re_c, defined by Equation 14.

$$Re_c = \frac{\omega R_p b}{\nu} \qquad \text{Eq. (14)}$$

Changenet and Velex [45] found that two regimes were required to accurately describe the experimental results, In the transition region between the two regimes, where $6000 < Re_c < 9000$, linear interpolation between the equations is used [45].

When modeling a gear pair, the formulae are used to determine the losses from each gear separately [45]. To account for the rotational direction dependence of churning losses due to the swell effect, where the rotation of the gears causes an increase in effective immersion depth in the vicinity of the pinion [45], an additional power loss determined from Equation 15 is added.

$$\Delta P = \frac{1}{2}\rho\omega^3 S_m R_p \Delta C_m \qquad \text{Eq. (15)}$$

where ΔC_m is the additional dimensionless churning torque, which is strongly dependent on the gear ratio G, determined from Equation 16 [45].

$$\Delta C_m = 17.7 Fr^{0.68} \cdot \frac{G-1}{G^8} \cdot \left[1 - \left(\frac{h}{R_p}\right)_{GEAR}\right] \qquad \text{Eq. (16)}$$

When applying this model to commercial two-stage EV transmission in Section 2.4, the two stages were treated separately, with only the second stage accounting for the swell effect. The immersion depth was assumed to be $6 \times m_n$ for

both stages. This is a gross simplification of the problem, as in reality, the movement of oil from one stage will affect the immersion depth of the other. The model was also developed for a splash-lubricated transmission, whereas, in the vehicle modeled in this paper, the first stage is, in fact, spray lubricated. This is likely to lead to reduced accuracy of the churning loss prediction in the first stage. Work is currently underway to develop improved churning loss models, and these will be substituted into the model when ready.

2.4. Application of the Model to a Real EV

The model was applied to a transmission installed in a current popular passenger EV. The gearbox architecture and component geometry in this transmission were measured and used as inputs to the model. A diagram of the internal transmission components is shown in Figure 6, with bearing locations indicated. Bearings 1-3, 5, and 6 are deep groove ball bearings, and Bearing 4 is a cylindrical roller bearing. A summary of the relevant gear parameters is shown in Table 1.

2.4.1. Thermal Coupling to the Environment

To predict transmission losses across a drive cycle, the ability to determine the evolution of sump temperature given the road conditions is crucial. An example of this temperature evolution is illustrated in Figure 7. Here, power losses and temperature rise predicted by the present model for a simple 1:1 spur gearbox running at a constant 200 Nm torque and 1500 rev/min speed are shown. The gearbox was treated as a lumped mass and heat loss from the gearbox was represented by a constant HTC from the casing to the surrounding air. The temperature rises from ambient (23°C) to a maximum of 43°C. The increase in oil temperature over time results in a significant increase in gear losses due to the reduction in lambda ratio resulting in gears operating further into the mixed lubrication regime. At the same time bearing losses decrease with time because bearings operate in full film throughout due to their lower roughness, and hence the decrease in film thickness in the full film regime reduces the hydrodynamic losses. There is a small decrease in churning losses due to the decrease in oil viscosity.

FIGURE 6 EV transmission layout as modeled in the present paper.

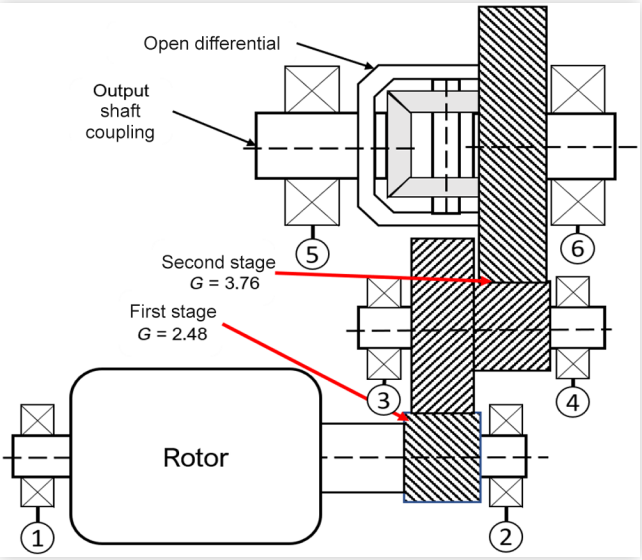

TABLE 1 Summary of EV gear parameters.

	Stage 1		Stage 2	
Parameter	Pinion	Wheel	Pinion	Wheel
Total gear ratio G_T	9.325			
Gear ratio G	2.48		3.76	
Tooth number z	31	77	21	79
Module m_n (mm)	1.7		2.62	
Facewidth b (mm)	30		39	
Profile shift x	0.12	0.12	0.16	0.04
Helix angle β (°)	20		22.5	

This sensitivity of losses to gearbox temperature means that it is critical to understand the heat transfers within the gearbox and to the surrounding environment. A relatively simple lumped mass model of the transmission was used to achieve this. The sum of the losses from the bearings, gear mesh, and lubricant churning at each time step is assumed to evenly heat the lumped mass of the transmission and oil. The specific heat capacity of this lumped mass was determined from that of the components and oil averaged by mass. As no side of the specific EV transmission modeled here is directly exposed to the airflow there is likely to be little heat transfer to the surroundings due to forced convection. Therefore, the majority of the heat out of the transmission is via active cooling by a stacked plate counterflow heat exchanger. Other routes of heat transfer from the transmission were neglected. The flow path of the oil through the transmission is shown in Figure 8.

A portion of the oil is sprayed onto the motor for cooling purposes. As the motor losses are significant, it is necessary to consider this additional heat transfer to the oil to accurately predict the oil sump temperature. The e-motor losses were estimated using the appropriate motor efficiency map.

The motor geometry was approximated as two concentric cylinders, representing the rotor and stator, separated by a long, narrow annulus of oil as shown in Figure 9(a). The ratio of the motor losses originating in the rotor and stator was assumed to be similar to the results of Wan et al. [51] for other permanent magnet synchronous motors.

The convective HTC within the annulus between the rotor and stator was estimated by using a Nusselt correlation for concentric rotating cylinders [52, 53]. The heat removed by the oil is calculated by determining the thermal resistance of mass transport (MT) using Equation 17 [36].

$$R_{MT} = \frac{1}{2\dot{m}c_p} \qquad \text{Eq. (17)}$$

Heat storage in the motor was analyzed using the lumped capacitance method.

FIGURE 7 An example prediction of the evolution of gearbox oil sump temperature and power losses for a simple 1:1 single-stage spur gearbox running at constant 1500 rev/min speed and 200 Nm torque over 4000 s.

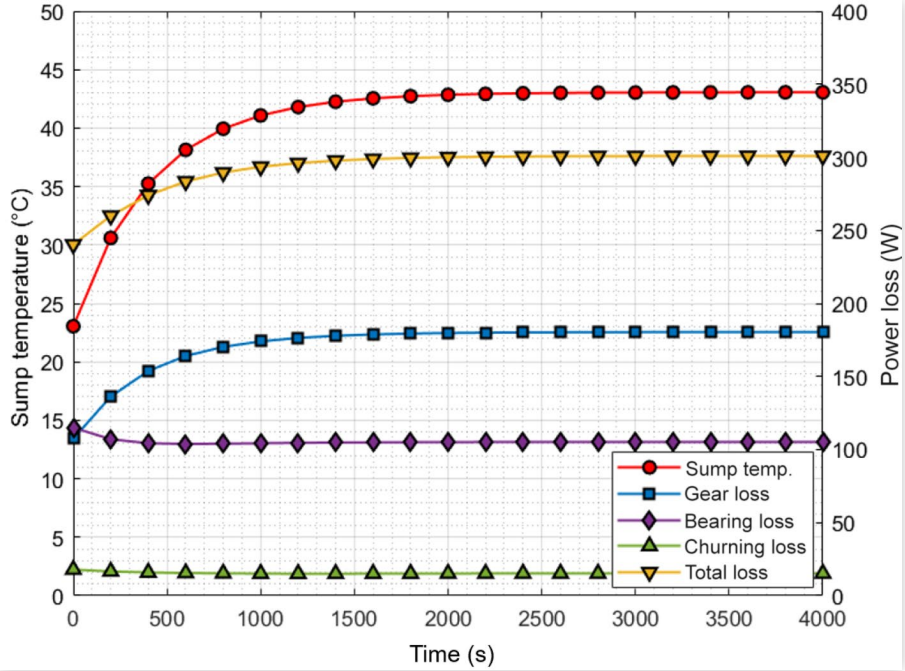

2.4.2. Heat Exchanger The heat exchanger is a stacked-plate counterflow heat exchanger. The external dimensions were measured from the disassembled transmission. The heat exchanger was analyzed using the effectiveness-NTU method [54].

The effective thermal properties of the lubricant and coolant within the heat exchanger were calculated using an iterative procedure. The coolant was assumed to be a 1:1 ratio mixture of ethylene-glycol and water. The properties of ethylene-glycol were taken from [54]. The HTCs within the exchanger were calculated from Nusselt correlations based on the hydraulic diameter of the channels and assumed thin channel walls with no fouling and fully developed flow within the channels.

FIGURE 8 An illustration of the oil flow through transmission in the example EV modeled here.

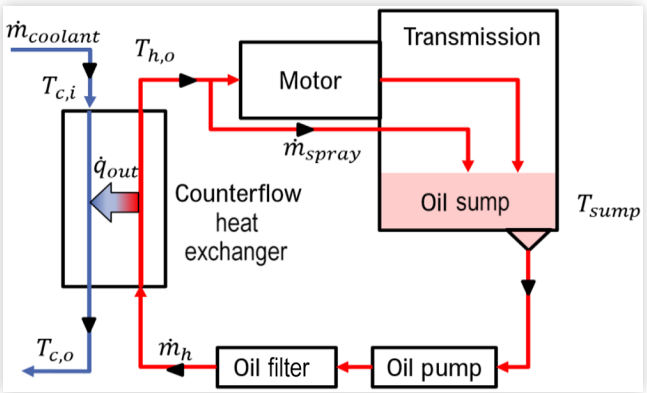

3. Determination of Lubricant Parameters

Several lubricant parameters are required for the implementation of the gear loss model. This section details the experimental determination of three key properties:

- Eyring stress
- z parameter
- Boundary friction

3.1. Eyring Stress and z Parameter

As described in Section 2.1, Eyring stress must be determined across a variety of temperatures and pressures to create a matrix. To do this, the approach developed by Lafountain et al. [48] successfully used in previous studies [2, 23, 55] was adopted. This method relies upon an approximation of Equation 1 to describe the relationship between strain rate, shear stress, and Eyring stress in the region prior to shear thinning and for $\tau > 1.5\tau_0$. This can be expressed by Equation 18:

$$\tau = \tau_0 \ln\left(\frac{2\eta_\rho \dot{\gamma}}{\tau_0}\right) \quad \text{Eq. (18)}$$

FIGURE 9 Motor thermal network used to predict the heat transfer to the oil during motor cooling.

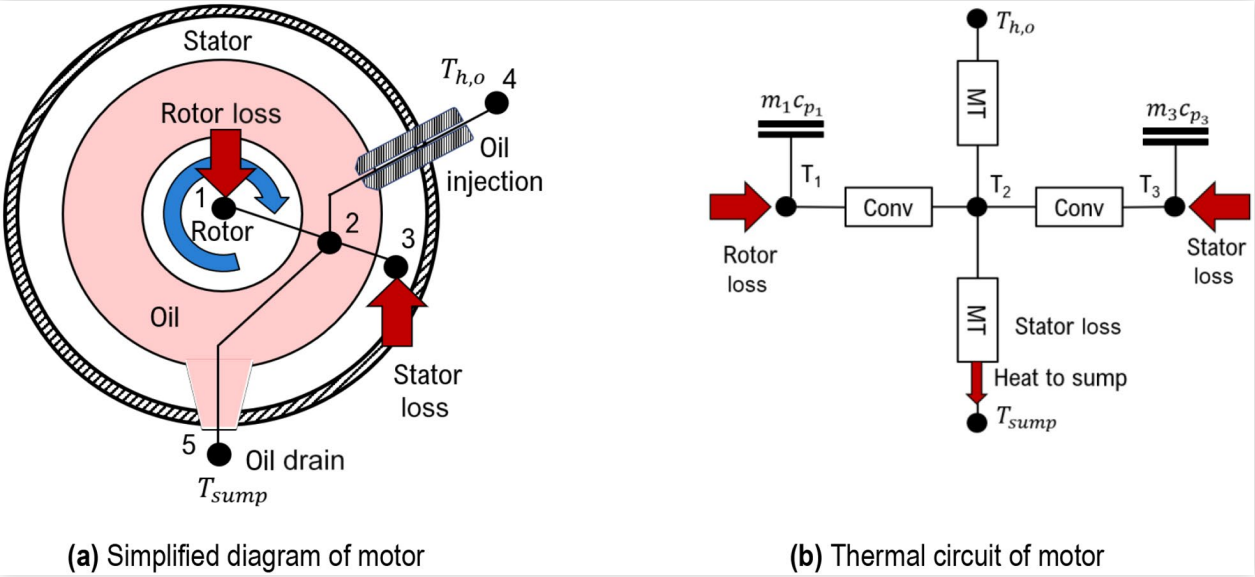

(a) Simplified diagram of motor **(b)** Thermal circuit of motor

This can be further expanded into the expression in Equation 19:

$$\tau = \tau_0 \ln(\dot{\gamma}) + \tau_0 \ln\left(\frac{2\eta_p}{\tau_0}\right) \quad \text{Eq. (19)}$$

Thus, plotting τ against $\dot{\gamma}$ on a logarithmic scale produces a straight line in this region with the gradient equal to the Eyring stress. By doing this using experimental data for several temperatures and pressures, interpolation can then be used to determine τ_0 at any other required temperature and pressure.

Once τ_0 is determined, the z parameter can be determined by curve fitting τ to $\dot{\gamma}$ using Equation 20, which is a combination of Equations 1 and 3.

$$\tau = \tau_0 \sinh^{-1}\left\{\frac{\dot{\gamma}}{\tau_0}\exp\left[\ln\left(\frac{\eta_r}{\eta_\infty}\right)\left(1+\frac{p}{p_r}\right)^z\left(\frac{T_r+135}{T+135}\right)^{S_0}\right]\right\} \quad \text{Eq. (20)}$$

3.1.1. Experimental Method To generate the required τ against $\dot{\gamma}$ plots, a series of tribometer tests were performed to create plots of the COF against SRR from which shear stress versus shear rate lots can be determined if the corresponding film thicknesses are additionally measured. Unlike in previous studies [23, 48, 55] which used the PCS Instruments Mini Traction Machine (MTM) ball-on-disc tribometer, a PCS Extreme Traction Machine (ETM) was used in this study for COF measurements. This was done as the MTM is only capable of applying a maximum Hertzian contact pressure of approximately 1.25 GPa using standard specimens. This limitation meant that it was necessary to extrapolate to obtain values for Eyring stress when contact pressures in gear teeth contacts exceeded this value. As the relationship between Eyring stress and pressure is highly nonlinear, this causes a great deal of uncertainty in the model results at high pressure. By using the ETM, which can apply up to 3.5 GPa with standard steel specimens, traction curves could be obtained at higher pressures and eliminate the requirement for extrapolation, thus making the gear lubrication model more accurate. A series of traction tests were performed at a variety of temperatures and loads. By adjusting the SRR and keeping the entrainment speed constant, tests were performed at various strain rates.

Tests were performed at an entrainment speed of 2700 mm/s, loads from 1.25 GPa to 2.68 GPa, and temperatures from 25°C to 145°C. To determine the strain rate in the above ETM tests, the lubricant film thickness at the relevant temperature and speeds was measured using the PCS Instruments optical EHD test rig. Since this rig uses a glass disc, the difference in film thickness resulting from the difference between the reduced elastic moduli between steel-steel and steel-glass contacts was compensated for by multiplying the measured film thickness by $\left(E^*_{\text{glass/steel}}/E^*_{\text{steel/steel}}\right)^{0.49}$, in line with the difference in film thickness predicted by Chittenden's [46, 47] equations.

Once τ and $\dot{\gamma}$ are calculated and plotted, the Eyring stress can be determined, as shown in Figure 10.

3.2. Boundary Friction

Since gears commonly operate in the mixed lubrication regime, the knowledge of the full film COF alone is not sufficient for the purposes of the present model. The expression shown earlier which estimates the mixed regime friction based on friction in full film and boundary regimes combined with the prevailing lambda ratio is used. The boundary COF of the lubricant was determined by performing a Stribeck test on an MTM using a rough disc ($Rq \approx 650$ nm) with a standard ball specimen. The rough disc was used to allow lower Λ ratios to be achieved at higher speeds than with standard specimens

FIGURE 10 An example of the fit for the Eyring stress obtained from ball-on-disc traction and film thickness measurements.

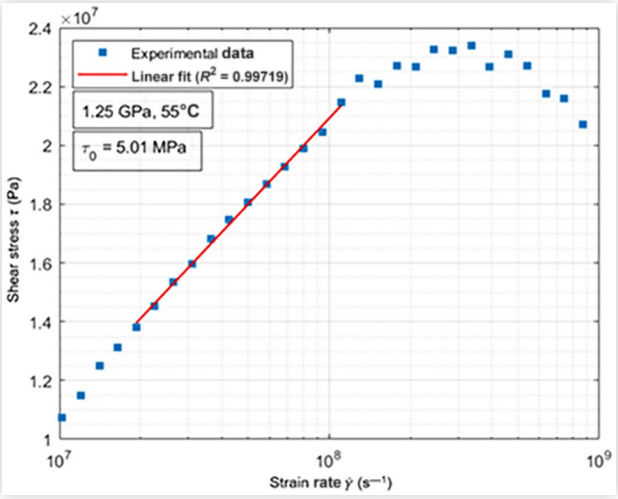

so that measurements can be made in the boundary regime. The roughness was measured before each test using a confocal microscope.

The boundary COF may change early in the operation of the gearbox due to wearing in and the formation of tribofilms on the metal surfaces. Therefore, a series of five Stribeck curves were produced. These were performed at a pressure of 0.86 GPa at 40°C with an SRR of 50% and rolling speeds from 10 mm/s to 2000 mm/s. A period of 30 min running at a constant rolling speed of 1000 mm/s separated each Stribeck curve. The spacer layer imaging method was used every 10 min in the first 30 min and every 30 min subsequently to monitor any tribofilm formation.

The boundary friction was taken from the final Stribeck curve as this allowed for wearing in and the formation of a tribofilm, and thus was deemed most representative of the value present in the gearbox for the majority of its lifetime.

4. Results

4.1. Comparison of the Model Predictions to Measurements Made in Real-World Road Tests

The validity of the model predictions was assessed by comparing the predicted evolution of oil sump temperature to measurements of this temperature made during real road tests with an EV with a transmission that is near identical to the one described in Section 2.4. As the exact properties of the synthetic ATF used in the vehicle during these tests were unknown, the synthetic fluid described in Section 4.2 was used for the model predictions as this has a similar base fluid of similar viscosity.

The vehicle was driven on a route incorporating urban and rural driving with hills. The route was driven first with the vehicle unloaded and then loaded with a 365 kg mass to vary the torque while keeping the speed approximately the same so that the model can be validated over a wider range of conditions. The torques and speeds across each drive cycle are shown in Figure 11.

The following inputs to the model were taken from measurements from instruments installed in the vehicle:

- Heat exchanger flow rates
- Coolant temperature at heat exchanger input
- Vehicle speed
- Motor torque

4.1.1. Prediction of Stator Temperature The validity of the thermal model of the heat exchanger and motor was determined by comparing the predicted stator temperatures to those measured by the vehicle's onboard instruments.

FIGURE 11 Speed and torque profiles in the experimental real road drive cycles. Ambient temperatures were measured as 3°C and 6°C in (a) and (b), respectively.

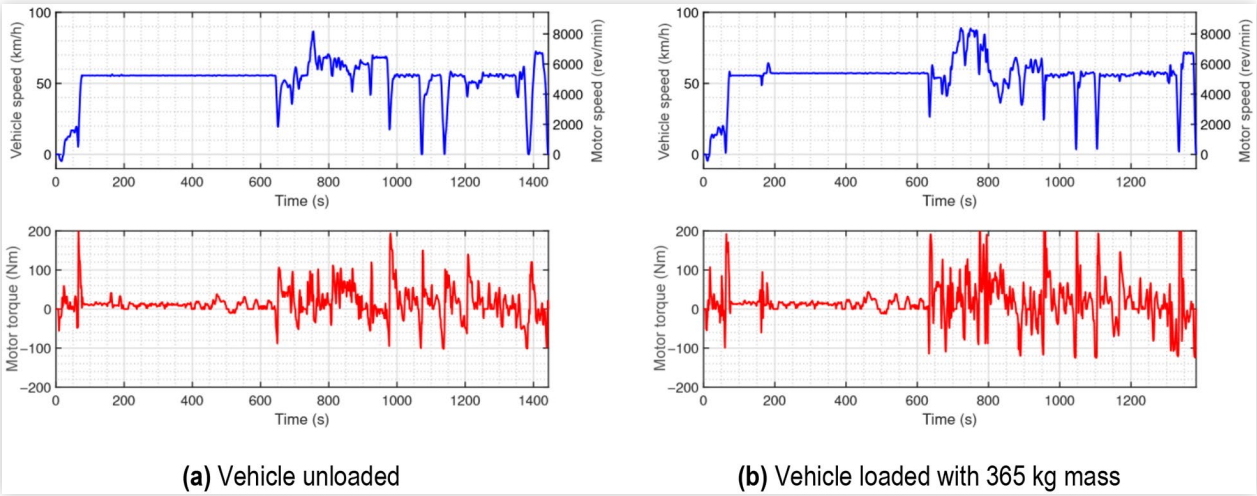

(a) Vehicle unloaded

(b) Vehicle loaded with 365 kg mass

FIGURE 12 Comparison of predicted evolution of stator temperatures to measurements made on a commercial passenger EV for two real-world drive cycles shown in Figure 11.

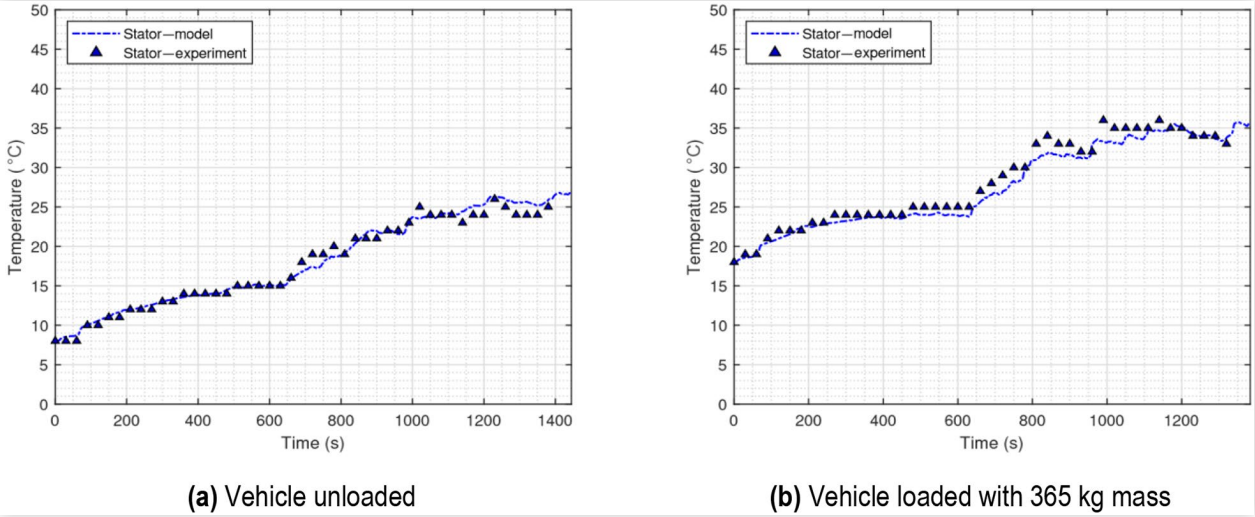

The oil temperature at the heat exchanger inlet was taken from experimental data rather than from the transmission model so that any error in the oil temperature prediction in the transmission would not affect the prediction of stator temperature.

As can be seen in Figure 12, the results of the model closely follow the experimental results, with R^2 values of 0.98 and 0.96 in Figure 12(a) and (b) respectively, instilling confidence in the reliability of the employed approach for the heat exchanger and oil-motor heat transfer predictions. This should ensure that the accuracy of the transmission loss predictions is not significantly impacted by the approximations used to model motor cooling.

4.1.2. Prediction of Sump Oil Temperature

The predicted oil sump temperatures from the simulations are compared to the measurements from the internal instruments of the vehicle in Figure 13. The model predicts the general trend of increasing sump temperature during the drive cycle well. The absolute values of temperatures are also relatively well predicted with the maximum temperatures reached at the end of the drive cycles being very close, although some discrepancies are seen during the earlier stages of the drive cycles.

It should be noted that the periods where the measured temperature appears constant are an artifact of the precision of the internal instruments of the vehicle.

FIGURE 13 Comparison of predicted evolution of oil sump temperatures to measurements made on a commercial passenger EV for two real-world drive cycles shown in Figure 11.

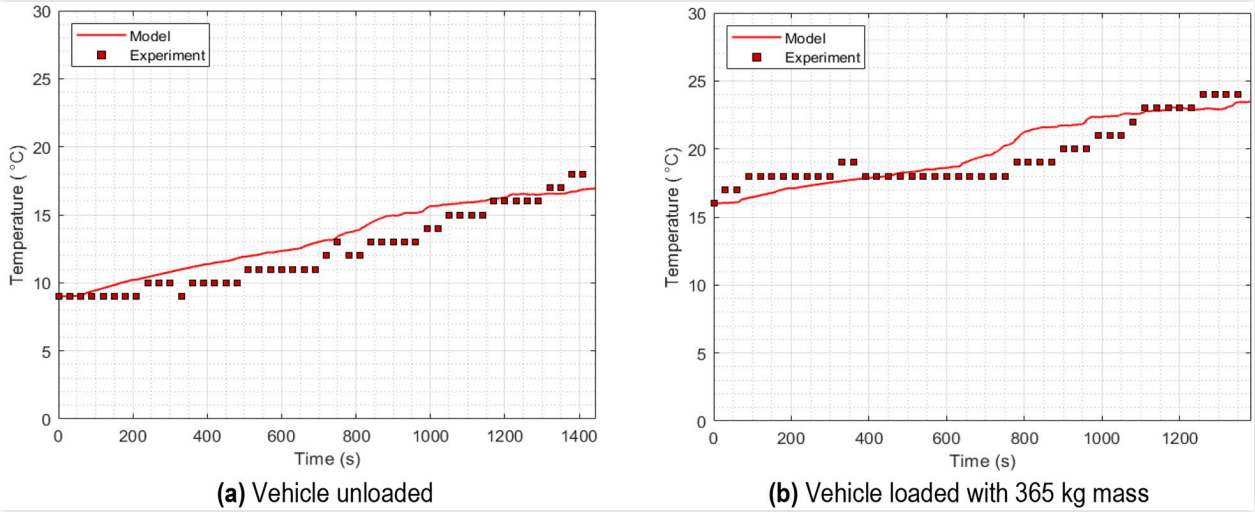

TABLE 2 Oil properties.

Parameter	Oil A	Oil B
Base oil	Mineral/Group III	PAO/Group IV
Additive package	ATF	ATF
$\nu_{40°}$ (cSt)	29.4	27.3
$\nu_{100°}$ (cSt)	5.90	5.90
VI (—)	155	174
k (W/(m·K))	0.136	0.141
$\alpha_{25°}$ (GPa^{-1})	2.45×10^{-8}	1.53×10^{-8}
μ_b (—)	0.118	0.130

4.2. Predicting the Impact of Lubricant Properties on EV Transmission Efficiency

To illustrate how the model may aid the selection and formulation of EV lubricants for improved transmission efficiency, the performance of two experimental ATFs was compared in the real EV transmission described above. The nominal properties of the oils are summarized in Table 2. Rheological properties and boundary COF were obtained using the aforementioned procedures.

4.2.1. Predicted Breakdown of Transmission Losses The model is able to predict contributions of individual losses in the transmission so that most inefficient components for the given conditions can be identified and optimized as needed. One way to analyze this breakdown of gearbox losses is to run the model at constant input power and increasing speed (and therefore decreasing torque) and constant sump temperature. The results of one such analysis for the modeled EV transmission are shown in Figure 14. The gearbox input power in these plots is 15 kW and the sump temperature is 30°C. The speed is shown on the main x axis while the corresponding input torque is shown on the secondary x axis on top of the plots. The input speed in these calculations was deliberately limited to 7000 rev/min to ensure that the $N{\cdot}d_m$ values of all bearings remained below the SKF bearing efficiency model speed limit of 0.5×10^6 mm-rev/min and also do not exceed the maximum speed of the tests used by Changenet and Velex [45] for their churning loss model employed here. For the modeled EV, a gearbox input speed of 1000 rev/min may, for example, translate to the vehicle driving at 10 km/h up a steep hill, while, at 7000 rev/min, the vehicle may be cruising at 72 km/h on a flat road.

It is immediately apparent that gear tooth friction losses are only significant at lower speeds and decrease as the speed, and hence film thickness in gear tooth contacts, increases. The gear churning losses, on the other hand, become significant at higher speeds only as may be expected. The bearing losses are important throughout and combined represent the biggest proportion of the overall loss, with the input shaft bearings being particularly important at high speeds. To analyze these bearing losses in more detail, the load-dependent and load-independent resistive torques from each bearing for the Oil A case are shown in Figure 15 separately for the input, intermediate, and output shaft. It should be noted that these plots show resistive torque, rather than power loss.

In Figure 15, it is clear that the resistive torque from load-dependent sources reduces with increasing speed and decreasing torque to an approximately constant value. Figure 15(a) shows load-independent resistive torque increases significantly with increasing speed, helping to explain the significant increase in losses with increasing speed from Bearings 1 and 2 seen in Figure 14.

4.2.2. Modeling Transmission Losses over the Whole WLTP Drive Cycle The present model was designed to be computationally efficient enough to assess the impact of the use of different lubricants and/or transmission

FIGURE 14 Predicted breakdown of transmission losses for the modeled EV gearbox with varying speed/torque at a constant power of 15 kW and constant oil sump temperature of 30°C.

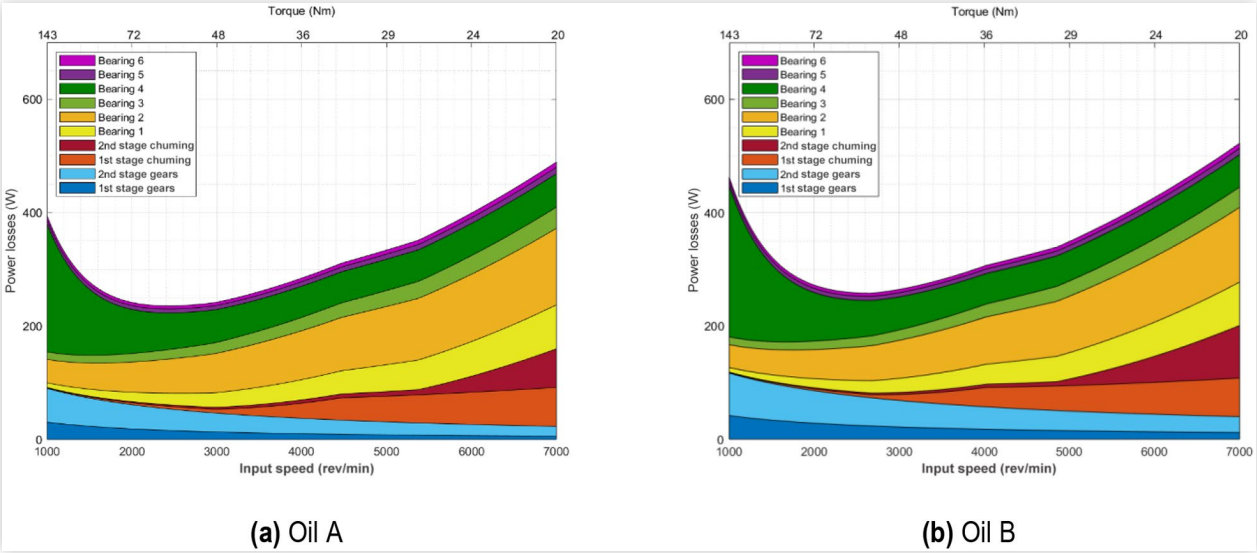

FIGURE 15 Load-dependent and load-independent resistive bearing torques on each shaft, normalized by the maximum total resistive torque for Bearing 4, at constant 15 kW power—Oil A.

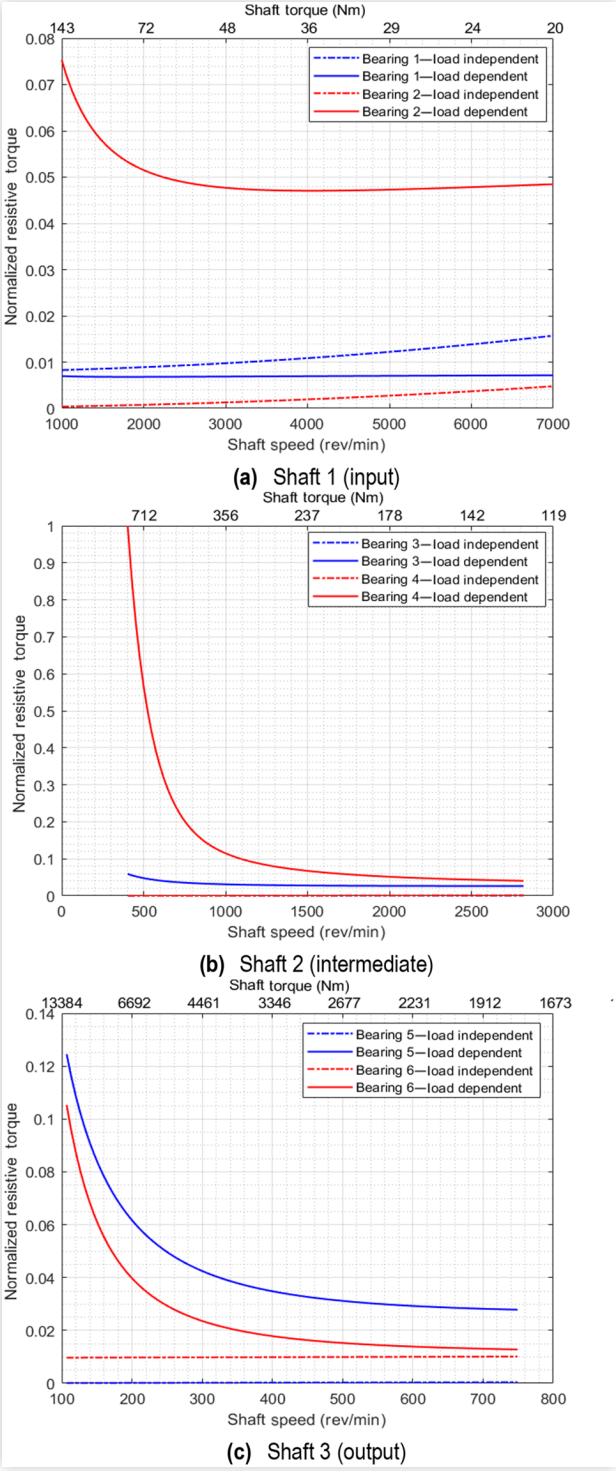

designs on transmission efficiency across entire standard drive cycles. This can be used to provide a useful indication of the effect of the selected lubricant on the vehicle range.

The performances of Oils A and B were compared across the Worldwide Harmonized Light Vehicles Test Procedure (WLTP) Class 3 drive cycle. This is a standard cycle used to assess EV range [56]. The predicted power losses over the course of the cycle for each oil normalized by the maximum predicted loss in each case are shown in Figure 16. It is clear that bearing losses are the most significant contributor to losses across the cycle. The contribution of churning losses is significant at high speeds while gears make up a smaller contribution. It should be noted that for much of the High and Extra High sections of the cycle, from 1000 s onward, the input shaft exceeds the maximum $N{\cdot}d_m$ value of the reliability of the SKF model, indicated by the dashed line in Figure 16, reaching a maximum of approximately 0.9×10^6 mm rev/min. Therefore, bearing drag losses are likely to be overestimated in these sections.

The predicted total energy lost to gear friction, bearing friction, and gear churning over the cycle using Oil A was 0.65, 1.02, and 0.95 times, respectively, than that of when using Oil B.

5. Discussion

5.1. Model Benefits and Limitations

The presented model provides a quick and effective way to quantitively evaluate the potential impact of different lubricants and/or gearbox architectures on EV gearbox efficiency. To achieve improved accuracy, the model requires just a few lubricant rheology parameters which can be obtained relatively easily using ball-on-disc test rigs following established procedures. These parameters allow the model to distinguish between the performances of two fluids with nominally similar properties. This is evident in Figure 16, where the sum of the gear losses across the WLTP cycle from Oils A and B differed by approximately 35%. This demonstrates that the consideration of nominal lubricant properties in isolation is insufficient to accurately predict the frictional behavior along the path of contact, highlighting the importance of the role played by lubricant rheology.

The comparisons of predicted oil sump temperature to experimentally measured values shown in Figure 13 illustrate that the model is able to predict relatively accurately the oil sump temperature, and hence power losses, over the conditions modeled here which were limited to speeds where the currently available relationships for the bearing drag and gear churning losses are valid. EV transmissions can operate at significantly higher speeds than this, and although the model can provide predictions at any speed, it is likely to overestimate losses at these higher speeds due to deficiencies in the existing bearing and gear churning loss models. This is discussed in more depth below. In the comparison of the model predictions to sump temperature measurements made on the loaded vehicle, shown in Figure 13(b), the recorded sharp increase in the oil temperature in the first 100 s of the drive cycle was evidently not captured by the model. This is likely due to the lumped mass approximation. The sump temperature predicted by the model and plotted here

FIGURE 16 Comparison of power losses with Oils A and B through WLTP Class 3 cycle. All power losses are normalized by the maximum total power loss reached during the cycle with Oil B.

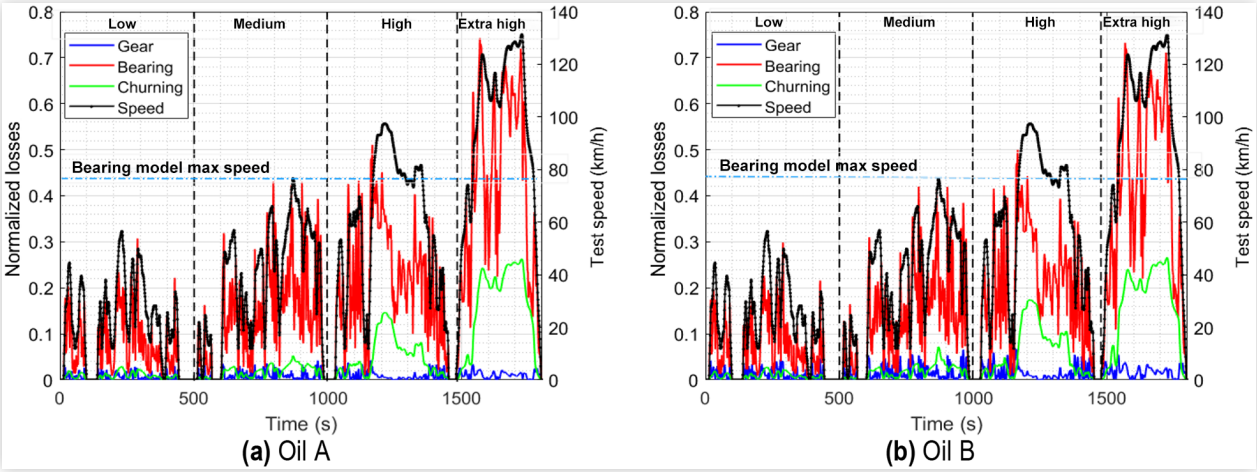

represents an average of all the transmission components rather than the oil temperature actually measured in a specific location in the sump. While the assumption provides a reasonable estimate, it inherently assumes that the components are heated evenly, and thus localized temperature increases are not captured. At higher speeds the accuracy of this approximation may be further decreased as enhanced convective heat transfer between the components and oil may lead to excessively high Biot numbers. Nonnegligible thermal gradients may also exist within the transmission, particularly in the vicinity of the bearings due to their significant power losses. Ongoing work to relax the lumped mass prediction indeed indicates that more accurate gearbox temperature predictions can be achieved by accounting for some of the temperature gradients inside the gearbox. The authors hope to report on this in the near future.

An important limitation to the accuracy of the gear tooth contact loss predictions is the approximation used to determine the gear HTCs. Given the complex geometry and operating environment consisting of a mixture of oil and air, it is extremely difficult to determine accurate HTCs for an operating gear. In such cases, HTCs are often obtained by fitting to experimental temperature measurements. However, measuring gear tooth temperatures during operation is just as difficult, hence the use of approximations in the present model. The approximations implemented here neglect features of the gear geometry which may act to enhance heat transfer. These include recesses in the gear sides and the profile of the gear teeth, which reduce the accuracy of the flat plate approximation used for the gear sides and the long cylinder approximation used for the gear track, respectively. In the track, heat transfer may be enhanced via the formation of recirculation regions between the teeth [50]. The rotary motion of the gear also causes heat transfer to occur over a range of length scales, and the teeth passing in and out of the sump results in two-phase cooling [50]. To address these issues, Chakravarthy and Kadiric [50] used a multiphysics approach to determine the HTCs between the gears and the sump, splitting the gear into a 2D gear to calculate the track HTC and a 3D disc to calculate the HTC for the sides. This showed that the track HTC obtained using current approximation may present an underestimate. While the multiphysics may well provide a more accurate estimate of HTCs, it requires extremely long computational times even for simple cases which render it undesirable for the purposes of the current model, which is intended to provide a relatively quick assessment of gearbox losses over a full drive cycle. However, if better estimates of the required HTC were obtained using multiphysics or other methods and tabulated, the current model is designed to be able to make use of such data.

Application of the model at high speed is currently limited by the uncertainties in the bearing drag and churning loss predictions. The SKF bearing loss model employed here is only designed to be used for bearing speeds below $N \cdot d_m = 5 \times 10^6$mm · rev/min; at higher speeds, it significantly overestimates the bearing drag losses [32, 33, 34]. The empirical fit for gear churning losses developed by Changenet et al. [45] as used here has only been validated with gear speeds up to 7000 rev/min. There is some evidence that churning losses may be limited at high speed, due to the oil being thrown around the gearbox, causing an effective reduction in immersion depth [37] and the reduction of bulk fluid motion in the vicinity of the gear [41]. Therefore, at high speeds the predictions of this model may overestimate gear churning losses when these conditions are met, but may underestimate them in other cases.

To illustrate the behavior of the current model at higher input speeds, comparisons of the sump temperature predictions of the model to measurements from the vehicle road tests on a highway, reaching a maximum speed of approximately 120 km/h, are shown in Figure 17. This maximum vehicle speed corresponds to $N \cdot d_m = 0.85 \times 10^6$ mm · rev/min for input shaft bearings, which is above the validity limit of the employed bearing loss model. The evident divergence between the predicted and experimental oil sump temperatures indicates a consistent overestimation of gearbox total power loss. The error accumulates over time as the predicted sump temperature drifts further from the true value, leading

FIGURE 17 An example of sump temperature predictions over a highway drive cycle where gearbox input speeds exceed the validity of the employed bearing loss and gear churning model.

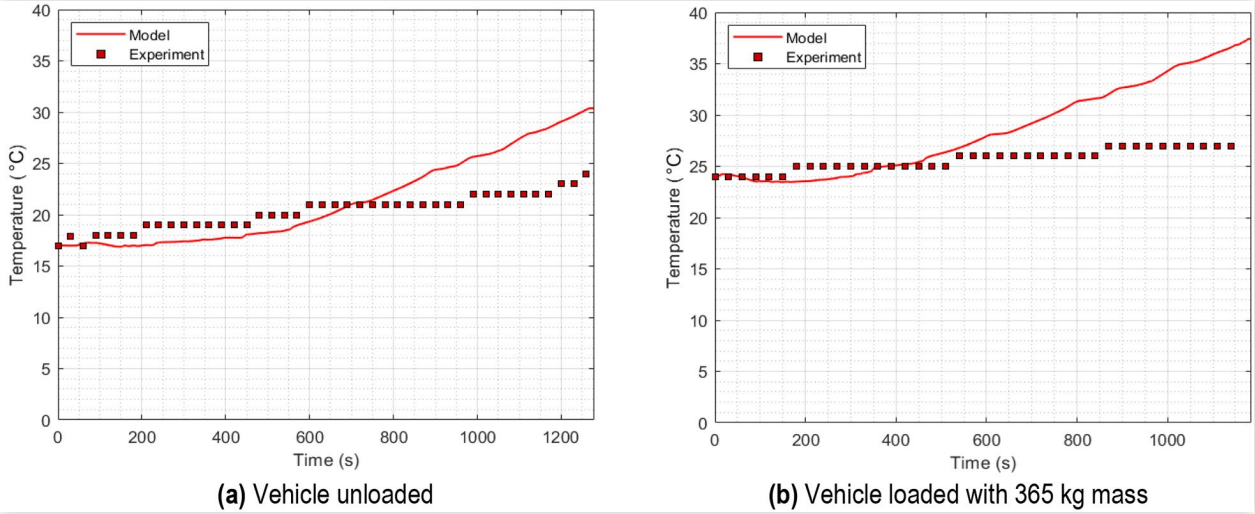

(a) Vehicle unloaded **(b)** Vehicle loaded with 365 kg mass

to inaccurate determination of the lubricant properties. To address these issues, work is currently underway to develop improved empirical fits for churning and bearing losses at higher speeds. Once available the updated models can be simply integrated into the overall transmission model.

5.2. Relative Contribution of Different Loss Sources to Overall EV Powertrain Loss

Under the conditions considered in Figure 14, the losses from the gearbox account for between approximately 1.5% and 3.3% of the constant 15 kW input power. Assuming the combined motor and controller efficiency of 90%, losses from the gearbox, therefore, account for between 13% and 25% of the total powertrain losses in this example. Comparing this to an ICE transmission, which only accounts for around 6.5% of the total powertrain losses in an ICE-powered vehicle [2], it is clear that investment into optimizing the transmission design and lubricant formulation is worthwhile for the purpose of EV range extension.

Figure 14 helps to identify the most significant individual loss contributions, in turn, indicating which aspects of the transmission design should be focused on most to improve the overall gearbox efficiency. Under the modeled conditions, bearing losses make the largest contribution to the overall gearbox loss, particularly at higher speeds. The most significant bearing losses come from Bearings 1, 2, and 4. The losses from Bearing 2 are high at all speeds, which are likely due to the Shaft 1 pinion being very off center, resulting in that bearing taking most of the radial load on Shaft 1. This is evident in Figure 15(a) where the load-dependent torque is an order of magnitude greater than the load-independent one for this bearing. Conversely, Bearing 1 has relatively high losses only at high speed and low torque, with the load-independent torque being of the same order of magnitude as the load-dependent torque at 1000 rev/min but twice as large at 7000 rev/min. The losses from the output shaft bearings are comparatively very low. These bearings operate at much lower speeds, and as such, the load-independent resistive torques are small. Figure 15(c) shows significant load-dependent torques from these two bearings as may be expected given their location. However, this does not translate to significant overall power loss due to the significantly lower speed of these bearings.

Gear churning losses are significant for the first stage for mid to high input speeds. The contribution from the second stage also becomes significant at higher speeds due to the influence of the swell effect. The linear interpolation between the results of Changenet and Velex's [45] two gear churning equations for the low- and high-speed range is visible in Figure 14(a), occurring between roughly 4000 rev/min and 5000 rev/min for the second stage. At 7000 rev/min, churning losses account for approximately 28% and 31% of the overall losses for Oils A and B, respectively, showing that churning losses can account for a significant proportion of overall losses under cruising conditions.

Figure 14 shows that gear tooth contact losses comprise a significant proportion of the overall transmission losses under low speed/high torque conditions due to low entrainment speeds resulting in lower lambda ratios. In the example modeled, at 1000 rev/min gear losses account for approximately 20% and 23% of the overall gearbox losses for Oils A and B, respectively. This reduces to 4% and 6% at 7000 rev/min. This indicates that although they are less significant than bearing losses, investment in designing for the minimization of gear losses could translate to significant vehicle range extension, particularly for EVs operating predominantly at lower speeds and under frequent stop-start conditions.

6. Conclusion

This paper presents a new model for the prediction of losses in a general automotive gearbox with a particular focus on transmission designs employed in EVs. The main features of the model are

- Thermal coupling between film thickness, gear tooth temperature, oil viscosity, oil rheology, and COF within the gear teeth contacts is accounted for using a thermally coupled gear lubrication model which employs an iterative procedure applied at multiple points along the path of contact.
- The gear loss model is complemented with empirical models of bearing and churning losses, thus predicting the total power losses in the entire gearbox.
- Experimentally derived rheological data is implemented when determining the EHL COF along the path of contact, allowing nominally similar lubricants to be differentiated. This is combined with measured values of boundary COF using a weighted average based on the lambda ratio. Thus, both the fluid properties and surface roughness of the gears are accounted for.
- In order to improve the accuracy of the model for EV applications specifically, the temperature evolution of the oil sump is predicted by considering heat generation from losses in the gearbox, together with the heat transfers associated with oil cooling the EM and heat removal via a heat exchanger.
- The model predictions of the sump temperature evolution are compared to measurements made in a real-world EV road test at low to medium vehicle speeds. The model predictions show good agreement with measurements.
- The model can be used to analyze power losses over the entirety of real or standardized drive cycles, thus making it useful in optimizing gearbox design and lubricant selection for improved vehicle efficiency and range.
- The main limitations of the current implementation of the model arise from the speed limitations of the employed bearing and gear churning loss models and from the treatment of the gearbox as a lumped thermal mass when determining temperature changes over a drive cycle.

The application of this model to a typical current EV transmission shows that

- Transmission losses can account for up to 15-25% of the overall EV power losses depending on operating conditions. This compares to only approximately 6% for an ICE vehicle, highlighting the importance of optimizing the lubricant formulation and gearbox design to improve EV efficiency and range.
- Overall, bearings losses are the greatest source of transmission power loss in the example EV transmission modeled here, with losses in the input shaft bearings being particularly significant. Churning losses account for a significant proportion of losses at higher speeds, while gear losses are significant at lower speeds.
- By incorporating measured lubricant rheology, model results show that two nominally similar EV transmission lubricants can produce different transmission losses; in particular, the total energy lost in the gear mesh itself over the WLTP cycle can vary by approximately 35% between the two lubricants. As gear mesh losses can account for around 20% of the total gearbox loss under high torque/low speed conditions, substantial improvements in transmission efficiency could be made by considering the rheology of the EV lubricant.
- The model provides an effective tool for optimization of EV lubricant selection and gearbox design, such as ratio split, gear geometry, and bearing selection for improved vehicle efficiency and range.

Acknowledgments

The authors would like to thank Tim Caudill for performing the EV road tests described in this paper.

Contact Information

Joseph Shore
Imperial College London
joseph.shore15@imperial.ac.uk

Nomenclature

$\boldsymbol{A}$ - Surface area (m^2)
$\boldsymbol{B_1}$ **and** $\boldsymbol{B_2}$ - Transient thermal resistance (K/W)
$\boldsymbol{b}$ - Facewidth (m)
$\boldsymbol{C_{ch}}$ - Churning torque (N · m)
$\boldsymbol{C_m}$ - Dimensionless churning torque
$\boldsymbol{c_p}$ - Specific heat capacity [J/(kg · K)]
$\boldsymbol{D_p}$ - Pitch diameter (m)
$\boldsymbol{D_0}$ - Deborah number
$\boldsymbol{E^*}$ - Reduced Young's modulus
$\boldsymbol{d_m}$ - Mean bearing diameter
$\boldsymbol{Fr}$ - Froude number
$\boldsymbol{G}$ - Gear ratio
$\boldsymbol{Ge}$ - Effective elastic shear modulus (Pa)
$\boldsymbol{h_c}$ - Central film thickness (m)
$\boldsymbol{k_{oil}}$ - Oil thermal conductivity [W/(m·K)]
$\boldsymbol{M}$ - Bearing frictional moment (N·m)
$\boldsymbol{M_{drag}}$ - Hydrodynamic drag frictional moment (N·m)
$\boldsymbol{M_{rr}}$ - Rolling resistance frictional moment (N·m)
$\boldsymbol{M_{seal}}$ - Seal frictional moment (N·m)
$\boldsymbol{M_{sides}}$ - Steady-state thermal resistance of gear sides (K/W)
$\boldsymbol{M_{sl}}$ - Sliding frictional moment (N·m)

M_{total} - Total steady-state thermal resistance of gear (K/W)
M_{track} - Steady-state thermal resistance of gear track (K/W)
M_1 **and** M_2 - Steady-state thermal resistance (K/W)
m_n - Gear module (m)
$\dot{m}$ - Mass flowrate (kg/s)
N - Rotational speed (rev/min)
p - Pressure (Pa)
p_r - Reference pressure (Pa)
$\bar{p}$ - Mean contact pressure (Pa)
$\dot{q}$ - Heat rate (W)
R_{MT} - Thermal resistance of mass transport (K/W)
R_p - Pitch radius (m)
Re - Reynolds number
Re_c - Critical Reynolds number
S_m - Immersed surface area (m^2)
S_0 - Atmospheric slope index
T - Temperature (K)
T_r - Reference temperature (K)
U - Entrainment speed (m/s)
U_s - Sliding speed (m/s)
V_0 - Oil volume (m^3)
z - Roelands equation parameter
α_0 - Hertzian contact half-width (m)
$\dot{\gamma}$ - Shear rate (s^{-1})
ΔC_m - Additional dimensionless churning torque
ΔP - Additional churning power (W)
η - Dynamic viscosity (Pa·s)
η_p - In-contact viscosity (Pa·s)
η_r - Reference viscosity (Pa·s)
η_0 - Inlet viscosity (Pa)
η_∞ - Viscosity constant (0.0000631 Pa·s)
Λ - Lambda ratio
μ - Effective COF
μ_b - Boundary COF
μ_f - Fluid COF
ν - Kinematic viscosity (m^2/s)
ρ - Oil density (kg/m^3)
τ - Shear stress (Pa)
τ_c - Critical shear stress (Pa)
τ_0 - Eyring stress (Pa)
$\overline{\tau_c^*}$ - Nondimensional limiting shear stress
$\overline{\tau}^*$ - Nondimensional average shear stress
ϕ_{ish} - Inlet shear heating reduction factor
ϕ_{rs} - Kinematic replenishment factor
$\psi_{1\text{-}7}$ - Churning loss model parameters
ω - Rotational speed (rad/s)

References

1. Sato, Y., Ishikawa, S., Okubo, T., Abe, M. et al., "Development of High Response Motor and Inverter System for the Nissan LEAF Electric Vehicle," SAE Technical Paper 2011-01-0350, 2011, https://doi.org/10.4271/2011-01-0350.
2. Kadiric, A. and Christodoulias, A., "A Model for Prediction of Gearbox Power Losses under Conditions Pertinent to EV Operation," Presentation at *Technische Akademie Esslingen 22nd International Colloquium Tribology*, Technische Akademie Esslingen, Esslingen, January 28-30, 2020.
3. Bottiglione, F., De Pinto, S., Mantriota, G., and Sorniotti, A., "Energy Consumption of a Battery Electric Vehicle with Infinitely Variable Transmission," *Energies* 7, no. 12 (2014): 8317-8337, https://doi.org/10.3390/en7128317.
4. Becker, E.P., "Gearboxes and Battery Electric Vehicles," *Tribol. Lubr. Technol.* 75, no. 8 (2019): 68.
5. Kwon, K., Jo, J., and Min, S., "Multi-Objective Gear Ratio and Shifting Pattern Optimization of Multi-Speed Transmissions for Electric Vehicles Considering Variable Transmission Efficiency," *Energy* 236 (2021): 121419, https://doi.org/10.1016/j.energy.2021.121419.
6. Laitinen, H., Lajunen, A., and Tammi, K., "Improving Electric Vehicle Energy Efficiency with Two-Speed Gearbox," in *2017 IEEE Vehicle Power and Propulsion Conference, VPPC 2017*, Belfort, France, 1-5, 2018, https://doi.org/10.1109/VPPC.2017.8330889.
7. De Pinto, S., Camocardi, P., Chatzikomis, C., Sorniotti, A. et al., "On the Comparison of 2- and 4-Wheel-Drive Electric Vehicle Layouts with Central Motors and Single- and 2-Speed Transmission Systems," *Energies* 13, no. 13 (2020): 3328, https://doi.org/10.3390/en13133328.
8. Liu, P., Feng, S., Wei, W., Gu, Y. et al., "Energy Consumption Analysis of a Novel Two-Speed e-Powertrain System for Electric Vehicle," in *Proceedings of the Energy Conversion Congress and Exposition—Asia, ECCE Asia 2021*, Singapore, 1801-1805, 2021, IEEE, https://doi.org/10.1109/ECCE-Asia49820.2021.9478972.
9. Wang, Y., Lü, E., Lu, H., Zhang, N. et al., "Comprehensive Design and Optimization of an Electric Vehicle Powertrain Equipped with a Two-Speed Dual-Clutch Transmission," *Adv. Mech. Eng.* 9, no. 1 (2017): 1-13, https://doi.org/10.1177/1687814016683144.
10. Tehrani, M.G., Kelkka, J., Sopanen, J., Mikkola, A. et al., "Transmission Configuration Effect on Total Efficiency of Electric Vehicle Powertrain," in *2014 16th European Conference on Power Electronics and Applications, EPE-ECCE Europe 2014*, Lappeenranta, Finland, 26-28, 2014, IEEE, https://doi.org/10.1109/EPE.2014.6910780.
11. Anderson, N.E. and Loewenthal, S.H., "Spur-Gear Efficiency at Part and Full Load," NASA Technical Paper 1622, 1980.
12. Petry-Johnson, T.T., Kahraman, A., Anderson, N.E., and Chase, D.R., "An Experimental Investigation of Spur Gear Efficiency," *J. Mech. Des. Trans. ASME* 130, no. 6 (2008): 0626011-06260110, https://doi.org/10.1115/1.2898876.

13. Michaelis, K., Höhn, B.R., and Hinterstoißer, M., "Influence Factors on Gearbox Power Loss," *Ind. Lubr. Tribol.* 63, no. 1 (2011): 46-55, https://doi.org/10.1108/00368791111101830.
14. Li, S. and Kahraman, A., "Prediction of Spur Gear Mechanical Power Losses Using a Transient Elastohydrodynamic Lubrication Model," *Tribol. Trans.* 53, no. 4 (2010): 554-563, https://doi.org/10.1080/10402000903502279.
15. Chang, L., Jeng, Y.R., and Huang, P.Y., "Modeling and Analysis of the Meshing Losses of Involute Spur Gears in High-Speed and High-Load Conditions," *J. Tribol.* 135, no. 1 (2013): 1-11, https://doi.org/10.1115/1.4007809.
16. AGMA 925-A03, "Effect of Lubrication on Gear Surface Distress-AGMA Information Sheet," January 2013.
17. Changenet, C., Oviedo-Marlot, X., and Velex, P., "Power Loss Predictions in Geared Transmissions Using Thermal Networks-Applications to a Six-Speed Manual Gearbox," *J. Mech. Des. Trans. ASME* 128, no. 3 (2006): 618-625, https://doi.org/10.1115/1.2181601.
18. Durand De Gevigney, J., Changenet, C., Ville, F., and Velex, P., "Thermal Modelling of a Back-to-Back Gearbox Test Machine: Application to the FZG Test Rig," *Proc. Inst. Mech. Eng. Part J: J. Eng. Tribol.* 226, no. 6 (2012): 501-515, https://doi.org/10.1177/1350650111433243.
19. Olver, A.V. and Spikes, H.A., "Prediction of Traction in Elastohydrodynamic Lubrication," *Proc. Inst. Mech. Eng. Part J: J. Eng. Tribol.* 212, no. 321 (1998): 321-332, https://doi.org/10.1243/1350650981542137.
20. Yu, Q., Chang, L., and Jeng, Y.R., "A Mathematical Model for Rolling/Sliding Line Contacts in Boundary and Near Boundary Lubrication," *Proc. Inst. Mech. Eng. Part J: J. Eng. Tribol.* 229, no. 11 (2015): 1279-1291, https://doi.org/10.1177/1350650115577115.
21. Spikes, H. and Zhang, J., "History, Origins and Prediction of Elastohydrodynamic Friction," *Tribol. Lett.* 56, no. 1 (2014): 1-25, https://doi.org/10.1007/s11249-014-0396-y.
22. Baglioni, S., Cianetti, F., and Landi, L., "Influence of the Addendum Modification on Spur Gear Efficiency," *Mech. Mach. Theory* 49 (2012): 216-233, https://doi.org/10.1016/j.mechmachtheory.2011.10.007.
23. Christodoulias, A., *Prediction of Power Losses in an Automotive Gearbox* (London: Imperial College London, 2017)
24. Fernandes, C.M.C.G., Marques, P.M.T., Martins, R.C., and Seabra, J.H.O., "Gearbox Power Loss. Part I: Losses in Rolling Bearings," *Tribol. Int.* 88 (2015): 298-308, https://doi.org/10.1016/j.triboint.2014.11.017.
25. Höhn, B.R., Michaelis, K., and Otto, H.P., "Influence of Immersion Depth of Dip Lubricated Gears on Power Loss, Bulk Temperature and Scuffing Load Carrying Capacity," *Int. J. Mech. Mater. Des.* 4, no. 2 (2008): 145-156, https://doi.org/10.1007/s10999-007-9045-z.
26. Hinterstoißer, M., Höhn, B.-R., and Michaelis, K., "Optimization of Gearbox Efficiency," *Goiiva i Maz. Časopis Za Tribol. Teh. Pod. i Primjen. Tekućih i Plinovitih Goriva i Inžinjerstvo Izgaranja* 48, no. 4 (2009): 462-480.
27. Diez-Ibarbia, A., del Rincon, A.F., Iglesias, M., De-Juan, A., Garcia, P. and Viadero, F. "Efficiency Analysis of Spur Gears with a Shifting Profile," *Meccanica* 51(3):707-723, 2016, https://doi.org/10.1007/s11012-015-0209-x.
28. Xu, H., *Development of a Generalized Mechanical Efficiency Prediction Methodology for Gear Pairs* (Columbus, OH: The Ohio State University, 2005)
29. Moss, J., Kahraman, A., and Wink, C., "An Experimental Study of Influence of Lubrication Methods on Efficiency and Contact Fatigue Life of Spur Gears," *J. Tribol.* 140, no. 5 (2018): 1-11, https://doi.org/10.1115/1.4039929.
30. Benedict, G.H. and Kelley, B.W., "Instantaneous Coefficients of Gear Tooth Friction," *ASLE Trans.* 4, no. 1 (1961): 59-70, https://doi.org/10.1080/05698196108972420.
31. Fernandes, C.M.C.G., Martins, R.C., and Seabra, J.H.O., "Coefficient of Friction Equation for Gears Based on a Modified Hersey Parameter," *Tribol. Int.* 101 (2016): 204-217, https://doi.org/10.1016/j.triboint.2016.03.028.
32. Niel, D., Changenet, C., Ville, F., and Octrue, M., "Thermomechanical Study of High Speed Rolling Element Bearing: A Simplified Approach," *Proc. Inst. Mech. Eng. Part J: J. Eng. Tribol.* 233, no. 4 (2019): 541-552, https://doi.org/10.1177/1350650117750806.
33. Morales-Espejel, G., "Using a Friction Model as an Engineering Tool," *Evol. SKF* 2 (2006): 27-30.
34. SKF, "The SKF Model for Calculating the Frictional Moment," 2017, 1-15, http://www.skf.com/binary/86-299767/TheSKFmodelforcalculatingthefrictionalmoment_tcm_12-299767.pdf.
35. Pouly, F., Changenet, C., Ville, F., Velex, P. et al., "Investigations on the Power Losses and Thermal Behaviour of Rolling Element Bearings," *Proc. Inst. Mech. Eng. Part J: J. Eng. Tribol.* 224, no. 9 (2010): 925-933, https://doi.org/10.1243/13506501JET695.
36. Pouly, F., Changenet, C., Ville, F., Velex, P. et al., "Power Loss Predictions in High-Speed Rolling Element Bearings Using Thermal Networks," *Tribol. Trans.* 53, no. 6 (2010): 957-967, https://doi.org/10.1080/10402004.2010.512117.
37. Achtenova, G. and Pakosta, J., "Estimation of the Gearbox No-Load Losses," SAE Technical Paper 2016-01-1092, 2016, https://doi.org/10.4271/2016-01-1092.
38. Wink, C.H., Marson, L., and Goyal, S., "Hybrid Analytical-Experimental Method to Map Power Losses of Automotive Transmissions over Their Operating Range," *Tribol. Int.* 143 (2019): 106070, https://doi.org/10.1016/j.triboint.2019.106070.
39. Kolekar, A.S., Olver, A.V., Sworski, A.E., and Lockwood, F.E., "The Efficiency of a Hypoid Axle—A Thermally Coupled Lubrication Model," *Tribol. Int.* 59 (2013): 203-209, https://doi.org/10.1016/j.triboint.2012.03.013.
40. Kolekar, A.S., Olver, A.V., Sworski, A.E., and Lockwood, F.E., "Windage and Churning Effects in Dipped Lubrication," *J. Tribol.* 136, no. 2 (2014): 1-10, https://doi.org/10.1115/1.4025992.
41. Leprince, G., Changenet, C., Ville, F., and Velex, P., "Investigations on Oil Flow Rates Projected on the Casing Walls by Splashed Lubricated Gears," *Adv. Tribol.* 2012 (2012): 1-7, https://doi.org/10.1155/2012/365414.
42. Lauster, E. and Boos, M., "Zum Wärmehaushal Mechanischer Schaltgetriebe für Nutzfahrzeuge," *VDI-Ber.* 488 (1983): 45-55.

43. Terekhov, A.S., "Hydraulic Losses in Gearboxes with Oil Immersion," *Russ. Eng. J. (English Transl. Vestn. Mashinostroeniya)* 55, no. 5 (1975): 7-11.
44. Changenet, C., Leprince, G., Ville, F., and Velex, P., "A Note on Flow Regimes and Churning Loss Modeling," *J. Mech. Des. Trans. ASME* 133, no. 12 (2011): 1-5, https://doi.org/10.1115/1.4005330.
45. Changenet, C. and Velex, P., "A Model for the Prediction of Churning Losses in Geared Transmissions—Preliminary Results," *J. Mech. Des. Trans. ASME* 129, no. 1 (2007): 128-133, https://doi.org/10.1115/1.2403727.
46. Chittenden, R.J., Dowson, D., Dunn, J.F., and Taylor, C.M., "A Theoretical Analysis of the Isothermal Elastohydrodynamic Lubrication of Concentrated Contacts. I. Direction of Lubricant Entrainment Coincident with the Major Axis of the Hertzian Contact Ellipse," *Proc. R. Soc. London, Ser. A (Mathematical Phys. Sci.)* 397, no. 1813 (1985): 245-269.
47. Chittenden, R.J., Dowson, D., Dunn, J.F., and Taylor, C.M., "A Theoretical Analysis of the Isothermal Elastohydrodynamic Lubrication of Concentrated Contacts. II. General Case, with Lubricant Entrainment along Either Principal Axis of the Hertzian Contact Ellipse or at Some Intermediate Angle," *Proc. R. Soc. London, Ser. A (Mathematical Phys. Sci.)* 397, no. 1813 (1985): 271-294.
48. Lafountain, A.R., Johnston, G.J., and Spikes, H.A., "The Elastohydrodynamic Traction of Synthetic Base Oil Blends," *Tribol. Trans.* 44, no. 4 (2001): 648-656, https://doi.org/10.1080/10402000108982506.
49. Smeeth, M. and Spikes, H.A., "The Influence of Slide Roll Ratio on the Film Thickness of an EHD Contact Operating within the Mixed Lubrication Regime," Presentation at the *Twenty-Second Leeds-Lyon Symposium on Tribology, the Third Body Concept*, Lyon, France, September 5-8, 1995.
50. Chakravathy, K. and Kadiric, A., "A New Thermally-Coupled Model for Prediction of Gearbox Power Losses," Presentation at the in *74th STLE Annual Meeting & Exhibition*, Nashville, Tennessee, May 19-23, 2019.
51. Wan, Y., Cui, S., Wu, S., and Song, L., "Electromagnetic Design and Losses Analysis of a High-Speed Permanent Magnet Synchronous Motor with Toroidal Windings for Pulsed Alternator," *Energies* 11, no. 3 (2018): 562, https://doi.org/10.3390/en11030562.
52. Fénot, M., Bertin, Y., Dorignac, E., and Lalizel, G., "A Review of Heat Transfer between Concentric Rotating Cylinders with or without Axial Flow," *Int. J. Therm. Sci.* 50, no. 7 (2011): 1138-1155, https://doi.org/10.1016/j.ijthermalsci.2011.02.013.
53. Tachibana, F. and Fukui, S., "Convective Heat Transfer of the Rotational and Axial Flow between Two Concentric Cylinders," *Bull. JSME* 7, no. 26 (1964): 385-391.
54. Incropera, F.P., Dewitt, D.P., Bergman, T.L., and Lavine, A.S., *Foundations of Heat Transfer*, 6th ed. (Singapore: John Wiley Sons, Inc., 2013), ISBN:978-0-470-64616-8.
55. Christodoulias, A.I., Olver, A.V., Kadiric, A., Sworski, A.E. et al., "The Efficiency of a Simple Spur Gearbox—A Thermally Coupled Lubrication Model," in *AGMA FTM 2014 American Gear Manufacturers Association Fall Technical Meeting, October 12-14, 2014*, Arlington, Virginia, 81-98, 2014.
56. WLTPfacts, "Getting Ready for WLTP," 2017, https://www.wltpfacts.eu/wp-content/uploads/2017/04/WLTP_Leaflet_FA_web.pdf, accessed February 19, 2021.

ISSN 0148-7191